

# LRSCLIP: A Vision-Language Foundation Model for Aligning Remote Sensing Image with Longer Text

Weizhi Chen, Jingbo Chen, *Member, IEEE*,, Yupeng Deng\*, Jiansheng Chen\*,  
Yuman Feng, Zhihao Xi, Diyou Liu, Kai Li, *Student Member, IEEE*, Yu Meng

**Abstract**—This study addresses the technical bottlenecks in handling long text and the “hallucination” issue caused by insufficient short text information in remote sensing vision-language foundation models (VLFM). We propose a novel vision-language foundation model, LRSCLIP, and a multimodal dataset, LRS2M. The main contributions are as follows: (1) By integrating multi-source remote sensing data and adopting a large language model labeling strategy, we construct the LRS2M dataset, which contains 2 million image-text pairs, providing both short and long texts for the first time, thus solving the problem of semantic granularity limitations in existing datasets; (2) The design of the LRSCLIP architecture based on Long-CLIP’s KPS module, which extends CLIP’s text processing capacity and achieves fine-grained cross-modal feature alignment through a dual-text loss weighting mechanism. Experimental results show that LRSCLIP improves retrieval accuracy by 10%-20% over the Long-CLIP baseline in the zero-shot long-text cross-modal retrieval task. For the zero-shot short-text cross-modal retrieval task, LRSCLIP achieves improvements over the current best model, GeoRSCLIP, with increases of 0.17%, 0.67%, and 0.92% in Text to Image R@1, Image to Text R@1, and mR on RSITMD, respectively, and 0.04%, 2.93%, and 1.28% on RSICD. In the zero-shot image classification task (average accuracy=75.75%) and semantic localization task (Rmi=0.7653), LRSCLIP achieves state-of-the-art performance. These results validate the dual advantages of fine-grained semantic understanding and global feature matching in LRSCLIP. This work provides a new benchmark model and data support for remote sensing multimodal learning. The related code has been open source and is available at <https://github.com/MitsuiChen14/LRSCLIP>.

**Index Terms**—Remote Sensing; Vision-Language Foundation model; Long Text; Multimodal Dataset; Zero-Shot Learning.

## I. INTRODUCTION

RECENT years have seen significant progress in foundation models (FM) within the fields of computer vision (CV) and natural language processing (NLP) [1] [2] [3] [4] [5] [6] [7] [8]. As a foundation model

\*Corresponding author: Yupeng Deng (dengyupeng@aircas.ac.cn), Jiansheng Chen (chenjs@aircas.ac.cn). This research was funded by the National Key R&D Program of China under grant number 2021YFB3900504.

Weizhi Chen, Kai Li are with Aerospace Information Research Institute, Chinese Academy of Sciences, Beijing 100101, China, and also with School of Electronic, Electrical and Communication Engineering, University of Chinese Academy of Sciences, Beijing 100049, China.

Jingbo Chen, Yupeng Deng, Jiansheng Chen, Zhihao Xi, Diyou Liu, Yu Meng are with Aerospace Information Research Institute, Chinese Academy of Sciences, Beijing 100101, China.

Yuman Feng is with the School of Information Network Security, People’s Public Security University of China, Beijing 100038, China.

that integrates both visual and language modalities, the vision-language foundation model(VLFM) [9] has injected new vitality into vision-language tasks. Unlike models designed for specific task objectives, VLFM learns joint representations of massive image-text pairs in upstream tasks and then transfers this knowledge to various downstream tasks, demonstrating exceptional performance. Several outstanding VLFM models have already emerged, such as CLIP [10], BLIP [11] [12], and MaskVLM [13]. Meanwhile, researchers have begun exploring the application potential of VLFM in the remote sensing domain. However, VLFM often faces issues related to the long-tail effect (where a small number of classes dominate while the rest have fewer samples), making direct application to remote sensing tasks challenging [14]. Consequently, transferring large-scale pre-trained knowledge from the general domain to the remote sensing domain has become the mainstream approach in adapting VLFM for remote sensing tasks. In line with this trend, several notable studies have emerged, such as RemoteCLIP [15], GeoRSCLIP [16], and GeoChat [17], offering valuable insights for remote sensing researchers. These tasks are typically addressed by fine-tuning the original foundational model with a small amount of remote sensing image-text data, enabling it to better adapt to typical tasks in the remote sensing domain, such as image classification [18], visual grounding [19] [20], semantic segmentation [21], change detection [22] [23], and visual question answering (VQA) [24], among others.

Currently, the language objects used for fine-tuning VLFM in the remote sensing field are mainly short texts. For example, commonly used remote sensing image caption datasets such as TextRS [25], RSICD [26], RSITMD [27], UCMerced [28], and Sydney-Captions [29] typically pair a remote sensing image with several short textual descriptions. If VLFM is fine-tuned using only such short text-remote-sensing-image pairs, two issues are likely to arise:

First, image captions in short texts generally provide only the main information of the remote sensing image, which may not be sufficient for remote sensing tasks, which require more detailed image descriptions. Unlike natural images, remote sensing images often present unstructured features that contain more objects, attributes, and their spatial relationships. However, short text captions usually cover only a brief summary. For example, in the RSICD [26] dataset shown in [Fig. 1](#), each image caption includes different primary land-cover objects, which may result in information loss when using a single

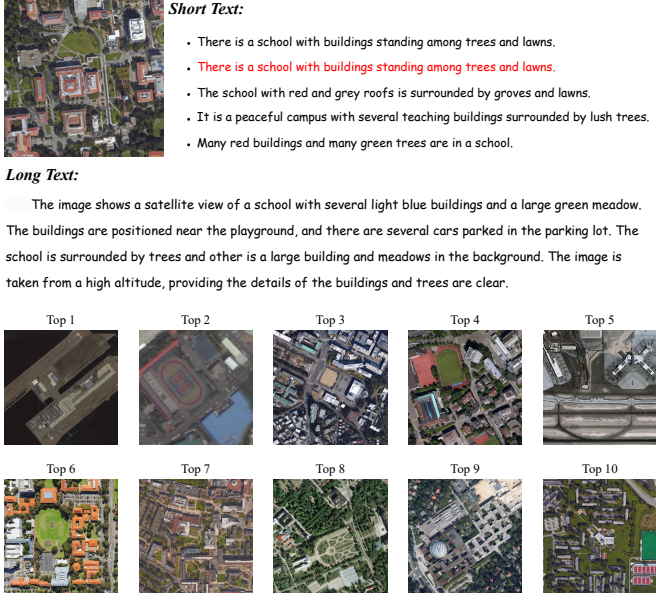


Fig. 1. Examples of short text image captions from RSICD and their corresponding long text captions from LRS2M, along with the top k retrieval results of GeoRSCLIP with red-font image captions.

sentence as a caption. Moreover, short text captions lack detailed descriptions, such as specific attributes of objects and the spatial relationships between them. For example, as shown in **Fig. 2**, when we use the sentence "A tennis court is located between two white buildings." to specifically query for a tennis court, LRSCLIP is able to focus most of the attention on the correct location. In contrast, GeoRSCLIP, which is trained with shorter text, tends to focus more on the tennis court object and overlooks its spatial relationship. This is reflected in the fact that, compared to LRSCLIP, GeoRSCLIP distributes attention across four other tennis court areas located at the bottom of the image.

Additionally, Liu et al. [15], and Zhang et al. [16] annotated image captions on several open datasets and used them to fine-tune CLIP in a supervised way, which improved performance in tasks like cross-modal retrieval and zero-shot classification. However, cross-modal retrieval tasks also reveal certain 'hallucination' issues within the model. As shown in **Fig. 1**, the Top 10 images retrieved for the red text exhibit some similarities. Subjectively, these Top 10 retrieval results mostly appear reasonable, which is partly due to the ambiguity between short text captions and remote sensing images, as well as domain-specific features. Wu et al. [30] suggested that longer image captions could significantly reduce the hallucination issue.

To address the above issues, training a VLFM with the ability to comprehend long texts is an ideal solution. However, current mainstream VLFMs, such as CLIP [10], generally have strict limitations on token lengths in text encoders. Furthermore, Zhang et al. [31] demonstrated that simply extending the maximum token length that CLIP can handle does not lead to a significant improvement in the image-text alignment. Their study also pointed out that CLIP's text encoder was primarily trained on short texts during the training phase, leading to insufficient training on higher-position tokens, which results

in an effective token length of approximately 20. To validate this conclusion, we conducted tests on GeoRSCLIP [16]. As illustrated in **Fig. 3**, when the text length exceeds 20-30 tokens, GeoRSCLIP's performance in terms of R@1 on both text-to-image and image-to-text tasks starts to plateau, in contrast to LRSCLIP. Additionally, we visualized the cross-attention under long text, as shown in **Fig. 2**. When the building token appears before the tennis court token, or vice versa, GeoRSCLIP is able to focus attention accurately on the former token but almost completely ignores the latter. The primary reason for this phenomenon is that GeoRSCLIP's training predominantly focuses on lower-level tokens, with insufficient training on higher-level tokens, making it difficult for the model to encode long text information effectively. Therefore, CLIP-based models not only face hallucination issues but also have limitations in handling long texts. Their ability to model long texts still requires improvement. In contrast, our LRSCLIP can accurately focus attention on the corresponding token regardless of the token's position.

In this study, we have developed a new remote sensing multimodal dataset, LRS2M, to facilitate the adaptation and transfer of general VLFM to remote sensing tasks. LRS2M integrates datasets like RS5M and VHM, containing approximately 2 million remote sensing image-text pairs. Unlike existing datasets, LRS2M provides short and long text captions, allowing the model to strengthen its long text understanding while still being able to interpret short text content precisely. Based on LRS2M, we trained LRSCLIP, a VLFM capable of handling long and short texts. By deeply aligning remote sensing images with long text representations, LRSCLIP is expected to improve fine-grained understanding of remote sensing scenes and dynamically utilize both global and local information based on task requirements, thus enhancing the model's cross-modal generalization capability.

In the practical application of VLFM, zero-shot learning (ZSL) [32] serves as a key indicator of the generalization ability of foundation models. The core idea of ZSL is to transfer learned knowledge to unseen categories or tasks without requiring additional labeled data, thereby significantly enhancing the model's adaptability and generalization. For remote sensing, new scenes and targets emerge continuously, and data annotation is costly. Therefore, VLFM with zero-shot capabilities is essential for intelligent remote sensing analysis. To comprehensively evaluate LRSCLIP's performance on zero-shot tasks, we designed four core evaluation tasks that cover key application scenarios, including cross-modal retrieval, classification, and semantic localization. First, the zero-shot long text cross-modal retrieval (ZCRL) task focuses on the model's ability to retrieve images in the context of long texts, while the corresponding zero-shot short text cross-modal retrieval (ZCRS) task assesses the model's performance in matching concise and incomplete textual descriptions. Additionally, the zero-shot image classification (ZIC) task evaluates the model's ability to recognize unseen categories, specifically testing whether it can classify images based solely on textual descriptions. Finally, the semantic localization (SeLo) task [33] focuses on cross-modal weak detection, where text semantics are used to localize relevant regions in images,

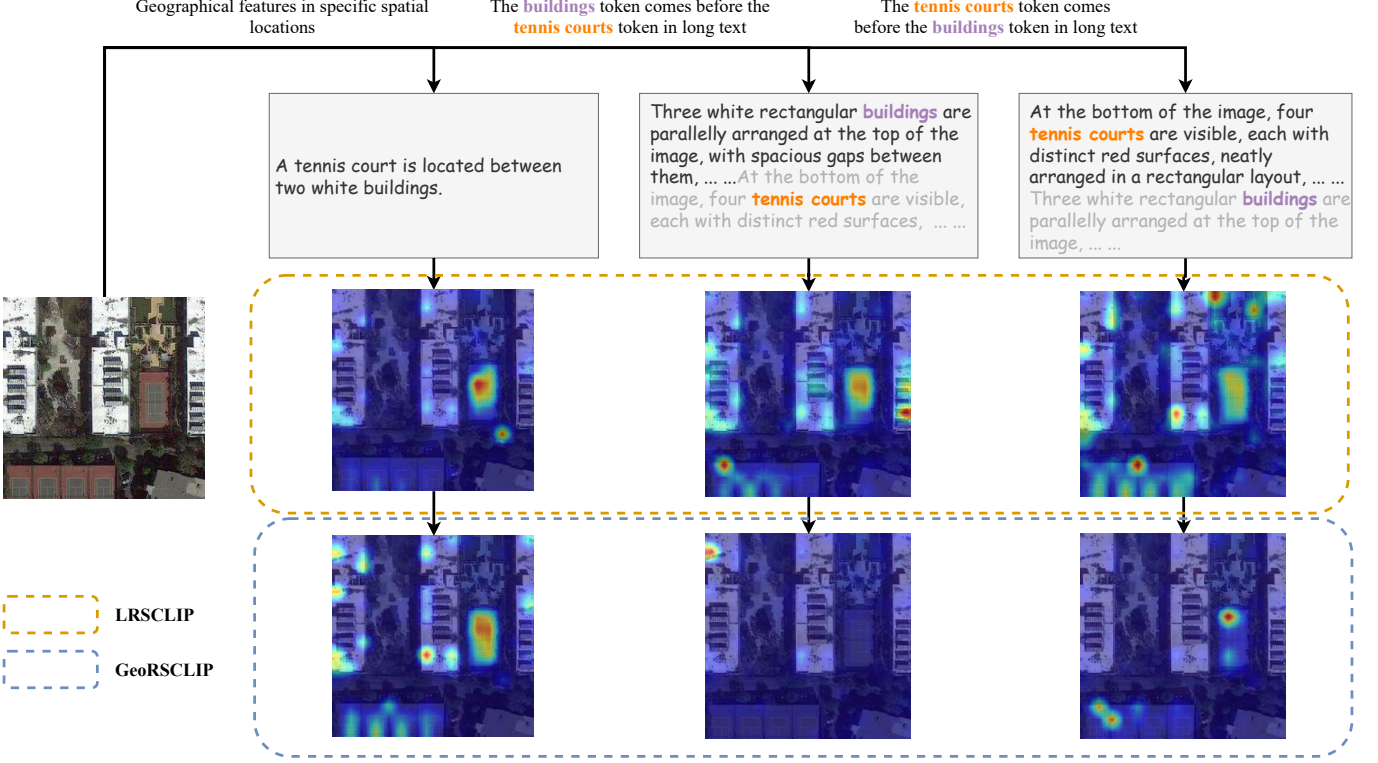


Fig. 2. Cross-attention heatmap visualization of remote sensing images using different text inputs in LRSCLIP and GeoRSCLIP.

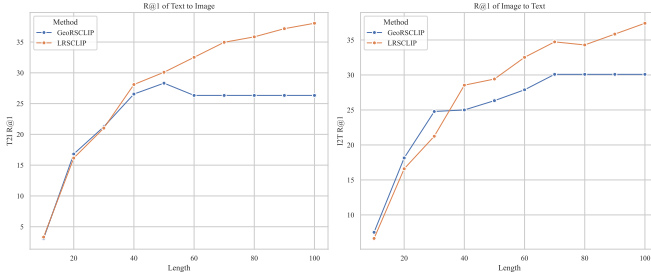


Fig. 3. Comparison of R@1 results for text-to-image and image-to-text retrieval tasks using different text lengths in GeoRSCLIP and LRSCLIP.

measuring the model's spatial semantic understanding and visual-language alignment ability.

Through a pre-training and systematic evaluation of downstream tasks, the results show that LRSCLIP excels in both long-text and short-text cross-modal tasks. It demonstrates significant improvements in fine-grained image understanding and shows good generalization in global semantic matching and zero-shot tasks. Compared to existing methods, LRSCLIP effectively overcomes the bottleneck caused by insufficient short-text information and inadequate long-text processing, providing a more flexible and precise solution for visual-language alignment in remote sensing scenarios. The following chapters will detail the construction of the LRS2M dataset, the architecture and training strategies of LRSCLIP, and the comprehensive evaluation and analysis of the model's performance across key tasks, including zero-shot cross-modal

retrieval, zero-shot classification, and semantic localization.

## II. RELATED WORK

### A. VLFM for Remote Sensing

The development of foundational theories in multimodal representation learning has laid an important foundation for VLFM research. By jointly encoding images and text, VLFM aims to construct a unified model architecture that efficiently integrates and understands information from both modalities. In recent years, with the introduction of large-scale pre-trained models like CLIP [10], VLFM applications have made breakthrough progress. These models leverage large-scale datasets for pre-training and demonstrate strong transfer learning abilities across various downstream tasks. In the remote sensing domain, images often have high resolution and diverse land-cover types, while textual descriptions contain rich semantic information related to these objects. VLFM bridges the semantic gap between images and text, opening up new possibilities for intelligent remote sensing data processing.

From a methodological perspective, VLFM research can be broadly divided into two main paradigms: contrastive learning and generative learning [34]. Contrastive learning-based VLFM enhances the semantic alignment between modalities by maximizing the similarity between images and text. Specifically, the model uses an image encoder and a text encoder to map images and text to a shared embedding space, using contrastive losses such as Triplet Loss [35] or InfoNCE Loss [36] to pull together correctly matched image-text pairs and push apart mismatched pairs. In contrast, generative learning-based

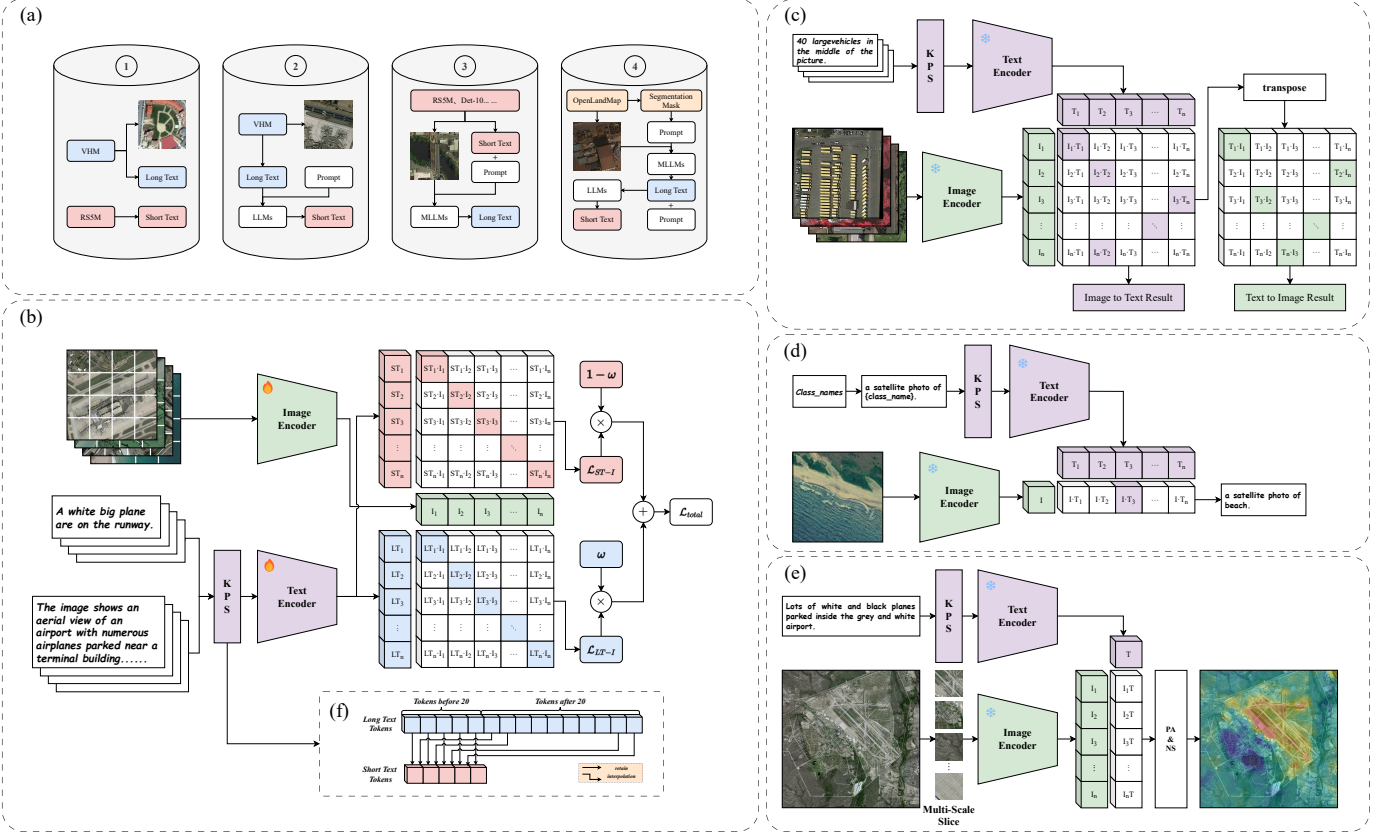


Fig. 4. Overview of LRSCLIP pipeline. (a) Four construction methods of LRS2M dataset. (b) Training process of LRSCLIP.  $\omega$  represents the weight of long text in the total loss. (c) Flowchart of ZCRL and ZCRS. (d) Flowchart of ZIC. (e) Flowchart of SeLo. PA&NS stands for Pixel-level Averaging & Noise Suppression. (c) Flowchart of KPS

VLFM focuses on generative tasks between images and text. For example, Muhtar et al. [37] combined multi-level vision-language alignment strategies with curriculum learning methods to generate contextually appropriate text descriptions and perform detailed reasoning.

CLIP [10] has used contrastive learning on 300 million image-text pairs to map images and text to a unified embedding space successfully. This has led to the development of several model variants, such as SigLIP [38], SLIP [39], Structure-CLIP [40], MaskCLIP [41], and CLIPPO [42]. These models have achieved outstanding performance in cross-modal retrieval and zero-shot tasks. However, since CLIP does not support tasks like object detection or visual grounding, researchers often need to design additional modules for integration. For example, Region-CLIP [43] enhances the pre-trained CLIP model with an R-CNN-style detector, enabling strong performance in open-vocabulary object detection tasks. CLIP-VG [44] implements visual grounding through a simple Transformer fusion module, and RISCLIP [45] treats the CLIP image and text encoders as backbone networks, introducing adaptive architectures for reference segmentation tasks.

Transferring CLIP from the general domain to the remote sensing domain presents a key challenge: creating suitable remote sensing datasets and building baseline models through supervised or task-specific fine-tuning. Studies like Remote-CLIP [15], SkyCLIP [46], and GeoRSCLIP [16] have fine-

tuned on customized image caption datasets while retaining the original CLIP architecture and have been evaluated on downstream tasks such as cross-modal retrieval and zero-shot classification. GeoRSCLIP achieved state-of-the-art semantic localization performance on the AIR-SLT [33] dataset. However, most of these studies focus on aligning short text captions with remote sensing images, primarily emphasizing local or salient features, while often lacking a deeper understanding of global and fine-grained information. Meanwhile, some studies have focused on aligning remote sensing images with geographic coordinates. For example, GeoCLIP [47] and SatCLIP [48] have fine-tuned the geographic coordinate encoding and image encoding in a contrastive manner similar to CLIP, successfully achieving tasks like Image-GPS retrieval.

### B. VLFM for Long Text Understanding

In traditional cross-modal retrieval systems, long texts are typically treated as a collection of short texts directly matched with images. However, long texts often contain rich semantic information, such as multiple land-cover categories, spatial relationships, and temporal context. This information must be fully extracted and organized to describe and match the corresponding images accurately. Contrastive learning models like CLIP are not designed to focus on long text processing. Their text encoders are usually limited to 77 tokens, which challenges aligning long texts with images.

To the best of our knowledge, existing VLMs have not yet fully addressed the challenges of understanding long texts in the remote sensing domain. However, some relevant explorations have gradually emerged in the general domain. The early DreamLIP [49] research randomly sampled sub-captions from detailed long text captions for training. While this approach somewhat improved the model's understanding of long texts, it did not fully utilize the complete long text information. Long-CLIP [31] expanded the text encoder's effective token length based on the original CLIP through methods like Knowledge Preserved Stretching (KPS) and Primary Component Matching (PCM). Additionally, it treated the first sentence of a long text (typically a summary or overview) as a short text input, maintaining good adaptation to short texts while enhancing long text comprehension. MATE [50] replaced the text encoder in VLM with a pre-trained encoder based on large language models (LLMs) and used multi-stage training to align the embeddings of images and LLMs, overcoming VLM's limitations in processing long captions or documents. LoTLP [30] re-annotated the data with long captions and incorporated corner annotations to integrate different types of textual information, thereby enhancing the model's ability to understand long texts while maintaining its performance on short text tasks. TULIP [51] extended CLIP's token processing capacity by using relative position distillation and relative position expansion, unlocking new possibilities for efficiently processing long texts.

### III. DATASET CONSTRUCTION

Manual annotation of remote sensing images with long text is not only time-consuming and labor-intensive, but also challenging, particularly when dealing with large-scale datasets. Annotators are required to provide detailed descriptions of the geographical information, environmental background, and topographical changes within the images. This process is susceptible to subjective variation, which can lead to reduced consistency and accuracy in the annotations. In contrast, utilizing multimodal large language models (MLLMs) can significantly improve annotation efficiency by automatically generating more consistent text descriptions, thus saving substantial time and costs.

However, a major challenge when using MLLMs for remote sensing image annotation is semantic bias. Most general-purpose MLLMs are pretrained on datasets from everyday domains, lacking the deep understanding of complex geographical information, environmental features, and high-dimensional spatial data inherent in remote sensing images. As a result, these models may fail to accurately capture the unique visual characteristics of the images, leading to discrepancies between the generated text and the actual content. For instance, as shown in **Fig. 5**, when generating instructions directly for an MLLM, the model may exhibit bias by incorrectly describing a "desert" scene as a "marble floor". To address this issue, we propose a prompt-guided generation strategy. Specifically, we incorporate already annotated image captions as prompts within the generation instructions to guide the model toward correct reasoning during the generation process. This strategy

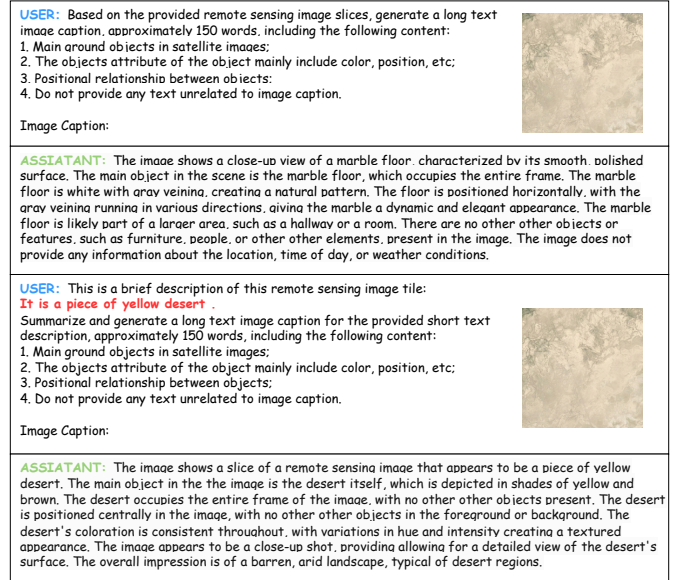


Fig. 5. The generated image captions of the MLLM under different generation instructions. The first generation instruction does not include the short text caption prompt of the image, while the second generation instruction includes the short text caption prompt of the image.

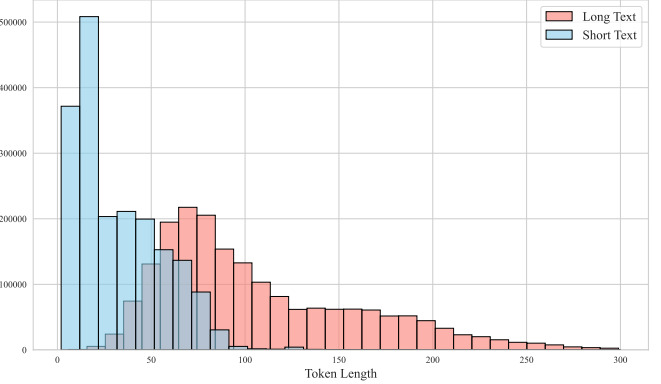


Fig. 6. Histogram of Token Length Distribution for Long and Short Texts.

enables the model to more accurately identify the scene in the remote sensing image, such as correctly recognizing and generating a description for a "desert" scene.

Based on this prompt-guided strategy, we have collected remote sensing image data from multiple open-source datasets, such as MillionAID [52], and combined it with long and short image captions annotated in datasets like VHM [53] and RS5M [16], or pixel-level label data for the images. These data will be used to construct a remote sensing image-text dataset, LRS2M, which includes both long and short text annotations.

As shown in **Fig. 4(a)**, the annotations in the dataset are divided into four categories based on the generation paradigm, forming a multi-dimensional and complementary annotation system. The first category of annotations is entirely based on open-source data integration by merging the long text annotations from VHM [53] for MillionAID [52] and the short text annotations from RS5M [16],

TABLE I  
DATA SOURCES FOR EACH SUBSET OF LRS2M AND THE AVERAGE TOKEN OF LONG AND SHORT TEXTS.

Dataset	Num	Long text Source	Long text Mean Tokens	Short text Source	Short text Mean Tokens
MillionAID [52]	920057	VHM [53]	77.39	RS5M [16]	20.73
CrowdAI [54]	276344	VHM [53]	91.57	Qwen2.5 [55]	36.74
CVACT [56]	44416	VHM [53]	82.39	InternLM2.5 [57]	39.14
CVUSA [58]	44416	VHM [53]	83.81	InternLM2.5 [57]	38.23
fMoW [59]	81224	VHM [53]	82.37	InternLM2.5 [57]	32.26
LoveDA [60]	23948	VHM [53]	83.00	GLM-4 [61]	39.14
BigEarthNet [62]	344385	Qwen2-VL [63]	195.66	RS5M [16]	65.77
Det-10 [15]	110794	Qwen2-VL [63]	174.40	Det-10 [15]	12.75
Seg-4 [15]	41171	LLaVA-OneVision [64]	179.53	Seg-4 [15]	14.56
UCMerced [28]	9430	LLaVA-OneVision [64]	207.17	UCMerced [28]	13.11
OpenLandMap	127533	Qwen2-VL [63]	171.10	Qwen2.5 [55]	45.42

920,057 high-quality benchmark pairs are created. The second category adopts a "long text guided generation" strategy. After obtaining long text annotations for CrowdAI [54], fMoW [59], CVACT [56], CVUSA [58], and LoveDA [60] from VHM [53], semantic compression and refinement are performed using InternLM2.5 [57], Qwen2.5 [55], and GLM-4 [61], resulting in 470,348 accurately matched short texts. The third category implements a "short text expansion generation" method. Based on short texts from RS5M [16], BigEarthNet [62], Det-10 [15] (which covers 10 detection datasets: AUAIR [65], CARPK [66], DIOR [67], DOTA [68], HRRSD [69], HRSC [70], LEVIR [71], RSOD [72], Stanford [73], Visdrone [74]), Seg-4 [15] (including 4 segmentation datasets: iSAID [75], LoveDA [60], Potsdam [76], Vaihingen [77]), and UCMerced [28], 481,555 long texts with spatial-semantic correlations are generated using the LLaVA-OneVision [64] and Qwen2-VL [63] multimodal models. The fourth category innovatively integrates object-level vector labels from OpenLandMap (The internal dataset of our research laboratory.), using them as semantic anchors for enhanced model understanding. Using LLaVA-OneVision [64] and Qwen2-VL [63], 127,533 text pairs are generated, possessing fine-grained features and global descriptive capabilities. The specific generation instructions and data format will be provided in [Appendix A](#).

We generated a total of 2,023,688 image-text pairs, forming the LRS2M dataset, where each image is associated with one long text and one short text. The average token lengths of the long text and short text are 110.89 and 32.36, respectively. **Table I** presents the statistics of each subset, and **Fig. 6** shows the token length distribution of the long and short texts. During the dataset construction, we designed a dual-text input mechanism by retaining both the long text and short text fields. This design allows the model to simultaneously learn the deep semantic features of long texts and the key information of short texts, thereby enhancing the model's ability to understand multi-granularity textual information.

## IV. LRSCLIP

### A. CLIP Architecture

The CLIP [10] proposed by OpenAI adopts a typical two-tower architecture. In this architecture, images and texts are processed through two independent encoders: one image encoder and one text encoder. The image encoder is typically a convolutional neural network (e.g., ResNet [78]) or a vision transformer (ViT) [79], while the text encoder is usually a Transformer-based model. These two encoders map the images and texts into a shared embedding space. Within this embedding space, CLIP optimizes the model using contrastive learning, ensuring that related image-text pairs are pulled closer, while unrelated pairs are pushed apart.

To implement this contrastive learning, CLIP employs a shared InfoNCE loss function. The goal of this loss function is to maximize the similarity between correctly paired images and texts, while minimizing the similarity between mismatched pairs (i.e., unrelated image-text pairs). For a batch of  $N$  samples, the mathematical expression of the InfoNCE loss function is as follows:

$$\mathcal{L}_{\text{InfoNCE}} = -\frac{1}{2N} \sum_{i=1}^N \left[ \log \frac{\exp(\text{sim}(v_i, t_i)/\tau)}{\sum_{j=1}^N \exp(\text{sim}(v_i, t_j)/\tau)} + \log \frac{\exp(\text{sim}(t_i, v_i)/\tau)}{\sum_{j=1}^N \exp(\text{sim}(t_i, v_j)/\tau)} \right] \quad (1)$$

where  $v_i$  represents the encoded feature vector of the  $i$ -th image,  $t_i$  represents the encoded feature vector of the  $i$ -th text, and  $\tau$  is the temperature parameter used to control the smoothness of the distribution. The function  $\text{sim}(v_i, t_i)$  represents the cosine similarity between the image and text, which is computed as:

$$\text{sim}(v_i, t_i) = \frac{v_i^\top t_i}{\|v_i\| \|t_i\|} \quad (2)$$

With this strategy, negative samples are not explicitly constructed, as in a batch of  $N$  samples, all pairs except the diag-

onal positive pairs are considered negative samples. Moreover, as the batch size  $N$  increases, the number of negative samples grows linearly, which contributes to improving the contrastive learning effectiveness.

### B. Knowledge Preserved Stretching

The token length of the text encoder in CLIP is strictly limited to 77, which leads to limitations in processing long texts and understanding fine-grained details of remote sensing images. Notably, simply extending the token length of the CLIP text encoder is insufficient to effectively improve image-text alignment. In this regard, the study of Long-CLIP [31] provides inspiration for our work. In the LRSCLIP architecture, we adopted the core module of Long-CLIP—Knowledge Preserved Stretching (KPS).

The KPS is a key solution proposed by Long-CLIP to address the position embedding length limitation of the CLIP text encoder. The basic idea is to preserve the first 20 well-trained position embeddings and use high-ratio interpolation to generate new position embeddings for the remaining positions. Experiments have shown that this strategy enhances the model's ability to process long texts while still maintaining good performance for short texts. The mathematical expression of this strategy is as follows:

$$PE^*(pos) = \begin{cases} PE^*(pos) & , \text{ if } pos < 20 \\ (1 - \alpha) \times PE \left( \lfloor \frac{pos}{\lambda} \rfloor \right) + \alpha \times PE \left( \lceil \frac{pos}{\lambda} \rceil \right) & , \text{ if } pos > 20 \end{cases} \quad (3)$$

where  $pos$  is the position index of the text token,  $\lambda$  is a large fixed interpolation ratio, and  $\alpha = \frac{pos\%}{\lambda}$ . As  $\alpha$  increases, the newly generated position embeddings approach those of the later embeddings.

Specifically, since most of the training text tokens in the original CLIP model are much smaller than 77, lower-position tokens are more thoroughly trained than higher-position tokens. Therefore, as verified by Zhang et al. [31], the practical maximum token length that CLIP can handle is 20. To avoid disrupting the absolute position representation of the text, we adopt a partial interpolation strategy. As shown in **Fig. 4(f)** and **Eq. (3)**, when  $pos \leq 20$ , the new position embedding  $PE^*(pos)$  directly retains the original position embedding  $PE(pos)$ . For  $pos > 20$ , interpolation is applied using the following equation:

$$PE^*(pos) = (1 - \alpha) \times PE \left( \lfloor \frac{pos}{\lambda} \rfloor \right) + \alpha \times PE \left( \lceil \frac{pos}{\lambda} \rceil \right) \quad (4)$$

This approach leverages the well-trained low-position embeddings while adjusting the high-position embeddings to better support long texts.

### C. Fine-tuning Based on CLIP

In the original design of the CLIP model, the input consists of a short text and an image, which is primarily suitable for aligning images with brief descriptions. To better capture the multi-level semantic relationships between images and texts, we propose extending the input of the CLIP model to include one long text, one short text, and one remote sensing image.

Specifically, as shown in **Fig. 4(b)**, we encode both the short text and long text through the same KPS and text encoder to obtain the embeddings of the long and short texts. These two embeddings are then aligned with the embeddings of the remote sensing image, which are obtained from the image encoder. The InfoNCE loss between the long text and the remote sensing image, as well as between the short text and the remote sensing image, is calculated using the **Eq. (1)**. The total loss is computed by:

$$\mathcal{L}_{total} = \omega \times \mathcal{L}_{LT-I} + (1 - \omega) \times \mathcal{L}_{ST-I} \quad (5)$$

where  $\omega$  is the loss weight for the long text and remote sensing image, with a value range of  $[0, 1]$ , and  $\mathcal{L}_{LT-I}$  and  $\mathcal{L}_{ST-I}$  represent the InfoNCE loss between the long text and remote sensing image, and between the short text and remote sensing image, respectively. Through this approach, the model not only learns the coarse-grained relationship between the short text and image, but also improves its fine-grained alignment ability by leveraging the richer contextual information provided by the long text.

Since CLIP has already learned general multimodal representations, fine-tuning allows the model to quickly adapt to the specific data distribution of remote sensing datasets. This has been validated in research in both the remote sensing [15] [16] and medical [80] domains. Furthermore, these studies have shown that full fine-tuning has an advantage over parameter-efficient fine-tuning like LoRA [81] when transferring to a specific domain. Therefore, we chose to fine-tune CLIP instead of pre-training it from scratch to build the LRSCLIP.

## V. EXPERIMENTS AND ANALYSIS

### A. Fine-tuning Setup

In this study, we selected two model sizes, ViT-B/16 and ViT-L/14, and performed full fine-tuning on the constructed LRS2M dataset. We adopted the tokenizer and KPS operation from Long-CLIP for text data processing, with the interpolation ratio set to 4. Thanks to KPS, the maximum token sequence length that LRSCLIP can handle is extended from the original CLIP's 77 to 248. Image data pre-processing follows the same strategy as Long-CLIP.

During training, each remote sensing image is paired with one short text and one long text, with a weight ratio of 8:2 for the InfoNCE Loss corresponding to the short text-image and long text-image pairs. This setup not only preserves the ability for short text retrieval but also introduces long text information, providing the model with more fine-grained multimodal alignment capabilities. Under this fine-tuning setup, we trained the model for one epoch on LRS2M using 8 NVIDIA 3090 GPUs. The optimizer settings are presented in **Appendix B**.

### B. Downstream Task Benchmark

We conducted four cross-modal tasks to evaluate the transfer and generalization capabilities of LRSCLIP, namely: Cross-modal Retrieval with Long text (ZCRL), Cross-modal Retrieval with Short text (ZCRS), Zero-shot Image Classification (ZIC) and Semantic Localization (SeLo). Among them, ZCRL and ZCRS are used to assess the cross-modal alignment of

long texts and short texts with remote sensing images, ZIC evaluates the zero-shot ability of LRSCLIP, and SeLo evaluates LRSCLIP’s fine-grained understanding and alignment of local information. The schematic diagrams for these four downstream tasks can be found in **Fig. 4(c) (d) (e)**.

**1) ZCRL:** As there is no existing baseline for Cross-model Retrieval with Long text in the remote sensing domain, we constructed the first such baseline, RSITMD-L and RSICD-L, based on the short text cross-modal retrieval datasets RSICD[18] and RSITMD[19], using Qwen2-VL[69]. The construction method is consistent with the third dataset construction method of LRS2M, where we used the short texts from RSITMD and RSICD as prompts for Qwen2-VL to prevent erroneous reasoning. The final RSITMD-L and RSICD-L datasets pair images with five short texts from the original dataset and one long text generated by Qwen2-VL. Based on LRSCLIP as the backbone, we conducted long text-to-image and image-to-long text retrieval tests on the RSICD and RSITMD test sets as divided by Liu et al. Evaluation metrics include recall@1/5/10 and mean Recall.

**2) ZCRS:** Similar to ZCRL, we used the same setup for short text-to-image and image-to-short text retrieval tasks on the RSICD and RSITMD test sets, with the same evaluation metrics of recall@1/5/10 and mean Recall.

**3) ZIC:** CLIP’s zero-shot image classification is achieved by embedding class names into prompt templates, such as “a photo of a {class\\_name}”. By matching images with prompts for each class, the one with the highest similarity is selected as the output category. Following CLIP’s prompt template, we use “a satellite photo of {class\\_name}” for our prompts and test on six scene classification datasets: RESISC45 [82], EuroSAT [83], PatternNet [84], WHU-RS19 [85], OPTIMAL-31 [86], and RS\_C11 [87] (including both training and testing sets). The evaluation metric is accuracy.

**4) SeLo:** Building on the work of Yuan et al. [33], we replaced LRSCLIP’s encoder with a backbone and conducted SeLo task testing on AIR-SLT. The evaluation metrics include:  $R_{su}$ : Measures the probability ratio between the ground-truth (GT) region and other regions. When the model focuses attention on the GT region, the value is close to 1; otherwise, it is close to 0.  $R_{as}$ : Quantifies the distance between the GT region center and the closest attention area. The value is close to 0 when attention is close to the GT center, and close to 1 when it is not.  $R_{da}$ : Measures the divergence of the model’s attention, which assesses retrieval model stability and whether the image contains the query target or relationship.  $R_{mi}$ : A composite measure incorporating the three above metrics:

$$R_{mi} = \omega_{su}R_{su} + \omega_{as}(1 - R_{as}) + \omega_{da}R_{da} \quad (6)$$

where  $\omega_{su} = 0.4$ ,  $\omega_{as} = 0.35$ ,  $\omega_{da} = 0.25$ . Except for  $R_{as}$ , all other metrics are better when higher.

To assess LRSCLIP’s performance across these downstream tasks, we compared it with CLIP[10], Long-CLIP[23], and remote sensing-based VLFM models GeoRSCLIP [16] and RemoteCLIP [15]. In the experimental results, CLIP and Long-CLIP represent VLFM models trained in the general domain, while GeoRSCLIP and RemoteCLIP are VLFM models trained on remote sensing short text tasks.

It is worth noting that LRSCLIP incorporates long text information during training, enabling it to focus on fine-grained local features. With this in mind, we chose ViT-B/16 to achieve finer image patch segmentation. However, since GeoRSCLIP and RemoteCLIP have not released pre-trained weights for ViT-B/16, we use their ViT-B/32 model as a benchmark. While this may introduce some unfairness, according to Zhang et al. [16], the performance difference between ViT-B/16 and ViT-B/32 is around 1%. To account for this difference, we treat this 1% as a correction factor. We also trained ViT-L/14 models to further validate and compare LRSCLIP’s performance at a larger size.

### C. Main Experimental Results

**TABLE. II** presents the experimental results of the ZCRL task, showing the performance of different model scales (ViT-B/16 and ViT-L/14) on the RSITMD-L and RSICD-L datasets. The results indicate that, compared to the general-domain Long-CLIP, LRSCLIP, fine-tuned on LRS2M, achieves significant improvements in both Text-to-Image and Image-to-Text retrieval tasks. Moreover, as the model size increases from ViT-B/16 to ViT-L/14, retrieval performance improves overall, with LRSCLIP still maintaining a clear advantage over Long-CLIP. These findings suggest that LRSCLIP, fine-tuned on LRS2M, is better suited for remote sensing image scenarios and outperforms Long-CLIP in cross-modal retrieval tasks.

**TABLE. III** summarizes the experimental results of the ZCRS task on the RSITMD and RSICD datasets, covering the retrieval performance of models with different sizes (ViT-B/16 and ViT-L/14). Since the pre-training dataset of RemoteCLIP includes RSITMD and RSICD, we did not include RemoteCLIP as a comparison for the ZCRS task. Overall, LRSCLIP, without additional learning on RSITMD and RSICD, significantly outperforms CLIP and Long-CLIP in retrieval performance. Specifically, on the base model, LRSCLIP outperforms GeoRSCLIP in Text-to-Image and Image-to-Text retrieval on the RSITMD dataset, with R@1 improvements of 0.71% and 2.43%, respectively, and 0.49% increase in the overall metric mR. On the RSICD dataset, while the Text-to-Image R@1 decreases slightly by -0.41%, the Image-to-Text R@1 and mR increase by 1.55% and 0.29%, respectively. After applying correction factors, LRSCLIP’s overall performance is comparable to GeoRSCLIP. On the larger-scale ViT-L/14 model, LRSCLIP shows slight improvements over GeoRSCLIP in R@1 and mR on RSITMD (0.17%, 0.67%, and 0.92%, respectively). On RSICD, the increases in R@1 and mR are more pronounced, reaching 0.04%, 2.93%, and 1.28%. In summary, LRSCLIP maintains strong performance on short-text retrieval while extending its capability for long-text modeling, demonstrating robustness and effectiveness in multi-length text scenarios without significant degradation compared to GeoRSCLIP, which is more focused on short-text retrieval.

**TABLE. IV** presents the experimental results of the ZIC task, including the accuracy on six datasets and the average accuracy. Overall, LRSCLIP achieves the highest average accuracy of 75.70 and 75.75 for the ViT-B/16 and ViT-L/14

TABLE II  
PERFORMANCE OF ZCRL ON RSITMD-L AND RSICD-L. THE PERFORMANCE OF LRSCLIP IS HIGHLIGHTED IN **BLUE**.

Testing Dataset	Size	Method	Text to Image			Image to Text			mR
			R@1	R@5	R@10	R@1	R@5	R@10	
RSITMD-L	ViT-B/16	Long-CLIP	19.03	51.33	71.02	18.14	51.33	71.02	45.43
		<b>LRSCLIP</b>	<b>38.50</b>	<b>73.89</b>	<b>84.96</b>	<b>36.28</b>	<b>70.80</b>	<b>84.29</b>	<b>64.79</b>
	ViT-L/14	Long-CLIP	24.12	59.29	77.88	17.70	50.44	65.93	49.23
		<b>LRSCLIP</b>	<b>39.16</b>	<b>72.12</b>	<b>87.39</b>	<b>35.62</b>	<b>70.58</b>	<b>85.40</b>	<b>65.04</b>
RSICD-L	ViT-B/16	Long-CLIP	11.89	31.93	46.20	7.96	25.53	39.43	27.15
		<b>LRSCLIP</b>	<b>23.15</b>	<b>51.51</b>	<b>66.61</b>	<b>20.22</b>	<b>47.67</b>	<b>63.68</b>	<b>45.47</b>
	ViT-L/14	Long-CLIP	14.91	36.87	52.52	6.77	24.70	38.52	29.05
		<b>LRSCLIP</b>	<b>26.72</b>	<b>55.54</b>	<b>70.45</b>	<b>21.96</b>	<b>48.95</b>	<b>66.42</b>	<b>48.34</b>

TABLE III  
PERFORMANCE OF ZCRS ON RSITMD AND RSICD. ZCRS DEMONSTRATES ITS ZERO-SHOT LEARNING ABILITY ON SHORT TEXTS, THEREFORE, IN THE COMPARATIVE EXPERIMENTS, WE DID NOT COMPARE WITH REMOTECLIP TRAINED ON RSITMD AND RSICD. PREVIOUS SOTA ARE INDICATED IN **RED**, AND THE PERFORMANCE OF LRSCLIP IS HIGHLIGHTED IN **BLUE**.

Testing Dataset	Size	Method	Text to Image			Image to Text			mR
			R@1	R@5	R@10	R@1	R@5	R@10	
RSITMD	ViT-B/32	CLIP	8.81	27.88	43.19	9.51	23.01	32.74	24.19
		GeoRSCLIP	14.16	42.39	<b>57.52</b>	19.03	34.51	46.46	35.68
	ViT-B/16	Long-CLIP	9.07	33.23	49.16	8.98	24.11	33.41	26.33
		<b>LRSCLIP</b>	<b>14.87</b>	<b>37.61</b>	<b>52.12</b>	<b>21.46</b>	<b>40.71</b>	<b>50.22</b>	<b>36.17</b>
	ViT-L/14	CLIP	10.13	31.64	46.24	10.84	28.10	36.50	27.24
		GeoRSCLIP	<b>17.35</b>	<b>41.46</b>	56.24	<b>20.35</b>	<b>38.05</b>	<b>49.56</b>	<b>37.17</b>
		Long-CLIP	12.74	36.99	53.27	11.28	27.43	38.50	30.04
		<b>LRSCLIP</b>	<b>17.52</b>	<b>41.68</b>	<b>56.73</b>	<b>21.02</b>	<b>39.38</b>	<b>52.21</b>	<b>38.09</b>
RSICD	ViT-B/32	CLIP	5.78	17.73	27.76	5.31	14.18	23.70	15.74
		GeoRSCLIP	9.52	27.37	40.99	11.53	28.55	39.16	26.18
	ViT-B/16	Long-CLIP	6.72	20.62	32.19	7.69	20.13	29.19	19.42
		<b>LRSCLIP</b>	<b>9.11</b>	<b>27.47</b>	<b>39.71</b>	<b>13.08</b>	<b>29.83</b>	<b>39.62</b>	<b>26.47</b>
	ViT-L/14	CLIP	4.96	18.72	29.66	6.59	17.75	28.09	17.63
		GeoRSCLIP	<b>9.97</b>	<b>28.18</b>	<b>42.10</b>	<b>12.72</b>	<b>28.82</b>	<b>41.17</b>	<b>27.16</b>
		Long-CLIP	7.14	23.48	35.55	8.78	20.40	28.82	20.70
		<b>LRSCLIP</b>	<b>10.01</b>	<b>28.60</b>	<b>43.73</b>	<b>15.65</b>	<b>31.38</b>	<b>41.26</b>	<b>28.44</b>

models, respectively, showing significant improvement over other methods. Specifically, compared to the general domain pre-trained CLIP and Long-CLIP, LRSCLIP outperforms them in accuracy on most datasets, demonstrating its advantages in remote sensing scenarios. Compared to GeoRSCLIP and RemoteCLIP, which is specifically trained for remote sensing short text tasks, LRSCLIP also achieves better or comparable zero-shot classification performance on most datasets, indicating that the introduction of long text information does not diminish its fine-grained discriminative ability. The results suggest that LRSCLIP has strong generalization capabilities in zero-shot image classification tasks.

TABLE. V presents the experimental results of the SeLo task on the AIR-SLT dataset, with SeLo-v1 [33] and SeLo-

v2 [88] as baselines. For both the ViT-B/16 and ViT-L/14 model sizes, LRSCLIP achieved the highest Rmi value, demonstrating more robust and precise localization capability. It is noteworthy that although Long-CLIP was not trained on any remote sensing data, its ability to process long texts still allowed it to outperform the original CLIP on most metrics, indicating that the inclusion of long texts helps the model better capture rich semantic information. GeoRSCLIP and RemoteCLIP, both trained with short texts, perform worse than LRSCLIP across all metrics, further demonstrating LRSCLIP's competitive advantage in focusing on target regions, suppressing irrelevant distractions, and achieving fine-grained alignment between remote sensing images and text.

TABLE IV

EXPERIMENTAL RESULTS OF ZIC ON SIX REMOTE SENSING IMAGE SCENE CLASSIFICATION DATASETS, WITH THE TEST DATA INCLUDING ALL SAMPLES FROM THE TRAINING AND TEST SETS OF EACH DATASET. PREVIOUS SOTA ARE INDICATED IN **RED**, AND THE PERFORMANCE OF LRSCLIP IS HIGHLIGHTED IN **BLUE**.

Size	Method	Testing Dataset						Mean
		RESISC45	EuroSAT	PatternNet	WHU-RS19	OPTIMAL-31	RS_C11	
ViT-B/32	CLIP	53.23	47.92	49.83	73.13	67.10	30.60	53.64
	RemoteCLIP	70.08	30.42	59.53	95.42	79.57	54.87	64.98
	GeoRSCLIP	72.82	58.99	<b>76.95</b>	72.82	82.69	57.63	70.32
ViT-B/16	Long-CLIP	61.83	51.57	58.68	80.50	72.04	58.20	63.80
	<b>LRSCLIP</b>	<b>73.12</b>	<b>57.55</b>	<b>74.30</b>	<b>87.16</b>	<b>85.27</b>	<b>76.79</b>	<b>75.70</b>
ViT-L/14	CLIP	61.57	24.73	61.32	82.29	67.10	47.48	57.41
	RemoteCLIP	<b>74.97</b>	39.07	63.48	<b>92.04</b>	81.99	<b>68.18</b>	69.95
	GeoRSCLIP	73.16	<b>61.77</b>	74.23	88.66	<b>82.80</b>	67.45	<b>74.68</b>
	Long-CLIP	65.79	61.33	70.37	87.16	76.34	57.87	69.81
	<b>LRSCLIP</b>	<b>75.30</b>	<b>58.17</b>	<b>76.61</b>	<b>88.26</b>	<b>86.18</b>	<b>69.97</b>	<b>75.75</b>

TABLE V

EXPERIMENTAL RESULTS OF SELO ON AIR-SLT. IN THE EVALUATION METRICS, EXCEPT FOR RAS, HIGHER VALUES ARE BETTER FOR ALL OTHER METRICS. PREVIOUS SOTA ARE INDICATED IN **RED**, AND THE PERFORMANCE OF LRSCLIP IS HIGHLIGHTED IN **BLUE**.

Size	Method	Semantic Localization(AIR-SLT)			
		Rsu	Ras	Rda	Rmi
—	SeLo-v1	0.6920	0.3323	0.6667	0.6772
	SeLo-v2	0.7199	0.2925	0.6658	0.7021
ViT-B/32	CLIP	0.7275	0.2878	0.7062	0.7168
	RemoteCLIP	0.7365	0.3008	0.6928	0.7125
	GeoRSCLIP	0.7546	0.2610	0.7180	0.7400
ViT-B/16	Long-CLIP	0.7508	<b>0.2405</b>	0.7369	0.7503
	<b>LRSCLIP</b>	<b>0.7689</b>	<b>0.2371</b>	<b>0.7345</b>	<b>0.7582</b>
ViT-L/14	CLIP	0.7318	0.3042	0.6514	0.6991
	RemoteCLIP	0.7727	0.2917	0.6834	0.7279
	GeoRSCLIP	0.7541	0.2513	<b>0.7573</b>	<b>0.7530</b>
	Long-CLIP	<b>0.7638</b>	0.2691	0.7297	0.7438
	<b>LRSCLIP</b>	<b>0.7803</b>	<b>0.2495</b>	<b>0.7620</b>	<b>0.7653</b>

#### D. Ablation Study

Unless otherwise stated, the evaluation metrics used in the ablation experiments for the ViT-B/16 LRSCLIP model on downstream tasks include the mean Recall (mR) for ZCRL, the mean Recall (mR) for ZCRS, mean accuracy for ZIC, and Rmi for SeLo.

**1) Influence of Batch Size:** [Fig. 7](#) illustrates the performance across various downstream tasks for batch sizes ranging from 64 to 512. Overall, larger batch sizes achieve better performance on the ZCRL, ZCRS, and ZIC tasks, which aligns with the needs of contrastive learning models using the InfoNCE loss function, as larger batch sizes provide a higher number of negative samples per iteration. This helps the network more effectively learn the contrastive features

between text and images. For the SeLo task, performance fluctuations are relatively small with changes in batch size, but there is still a slight improvement at the maximum batch size, indicating that larger batch sizes can also enhance the localization robustness in weak detection scenarios. In conclusion, selecting an appropriately large batch size can improve model performance across multiple remote-sensing cross-modal tasks.

**2) Influence of LRS2M Subset Size:** We trained the model using subsets of the LRS2M dataset with sizes of 0.5M, 1M, 1.5M, and 2M, and evaluated the performance on the ZCRL, ZCRS, ZIC, and SeLo tasks. As shown in [Fig. 8](#), overall, with the increase in training data size, the performance (mR) on the ZCRL and ZCRS tasks tends to improve, with the 2M

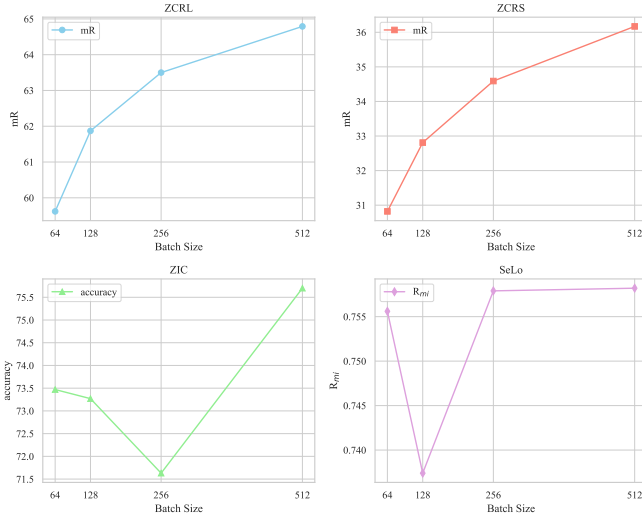


Fig. 7. Influence of Batch Size.

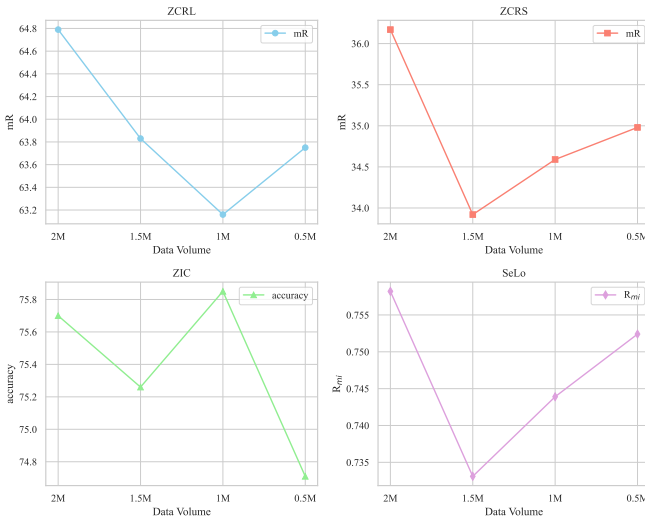


Fig. 8. Influence of LRS2M subset size.

dataset achieving the best performance. For the ZIC task, the accuracy of the 1M and 2M datasets is similar, while for the SeLo task, the largest 2M dataset also achieved the highest  $R_{mi}$  value. This suggests that, under the contrastive learning framework, leveraging a larger number of multimodal samples typically improves remote sensing image-text alignment and fine-grained retrieval performance. However, certain tasks or metrics may exhibit local fluctuations on smaller datasets due to training differences or random factors. Overall, the 2M dataset size provides relatively optimal performance across multiple tasks.

**3) Influence of Using PCM:** In this experiment, we investigate the impact of the PCM (Fine-tuning with Primary Component Matching) strategy on model performance. During training, this strategy aligns the long text encoding directly with the image encoding while aligning the primary components of the short text encoding with the image encoding. As shown in **TABLE. VI**, with PCM enabled, the mR for

TABLE VI  
INFLUENCE OF USING PCM

PCM	ZCRL	ZCRS	ZIC	SeLo
True	67.63	37.29	74.44	0.7478
False	64.79	36.17	75.70	0.7582

ZCRL reached 67.63, showing an improvement over the results without PCM, indicating that PCM significantly enhances the alignment between long text and images. Although the performance on ZCRS is similar whether PCM is enabled or not, the results for ZIC and SeLo tasks were slightly better without PCM. This may be due to information loss caused by the PCA transformation, which altered the image encoding's original feature distribution required for these tasks. Overall, PCM improves cross-modal retrieval performance but does not necessarily bring benefits for zero-shot classification and semantic localization tasks, which require richer visual features, highlighting the varying demands of different downstream tasks on the encoding space.

TABLE VII  
COMPARISON OF DOWNSTREAM EXPERIMENTAL RESULTS BETWEEN THE SHORT TEXT AND LONG TEXT PARTS OF LRS2M TRAINED WITH THE CLIP ARCHITECTURE AND LRSCLIP.

Method	Training Dataset	ZCRL	ZCRS	ZIC	SeLo
CLIP	LRS2M-S	45.59	29.09	62.19	0.7195
CLIP	LRS2M-L	55.38	30.52	65.55	0.7399
LRSCLIP	LRS2M	64.79	36.17	75.70	0.7582

**4) Influence of Using Different Model Frameworks:** We trained the CLIP framework on the LRS2M-S (which only includes short texts) and LRS2M-L (which only includes long texts) datasets and compared the results with those obtained from training LRSCLIP on the full LRS2M dataset. The results in **TABLE. VII** indicate that when CLIP is trained on LRS2M-S alone, its performance on various tasks is relatively lower. However, when trained on LRS2M-L, all tasks show significant improvements, demonstrating that long text provides richer semantic information for the model. Nevertheless, when trained on the complete LRS2M dataset, Long-CLIP's performance further improves and significantly outperforms the CLIP models trained on only one type of text. This suggests that leveraging both short and long text information simultaneously yields more substantial benefits in multimodal alignment and semantic understanding.

**5) Influence of Model Size:** **Fig. 9** presents the results of downstream tasks using LRSCLIP with different model sizes. Within the same ViT model size, patch size plays a critical role in the fine-grained representation of remote sensing images. Specifically, when switching from ViT-B/32 to ViT-B/16, except for a slight decrease in mR for RSICD-L, the performance of other downstream tasks significantly improves. This indicates that more granular image partitioning

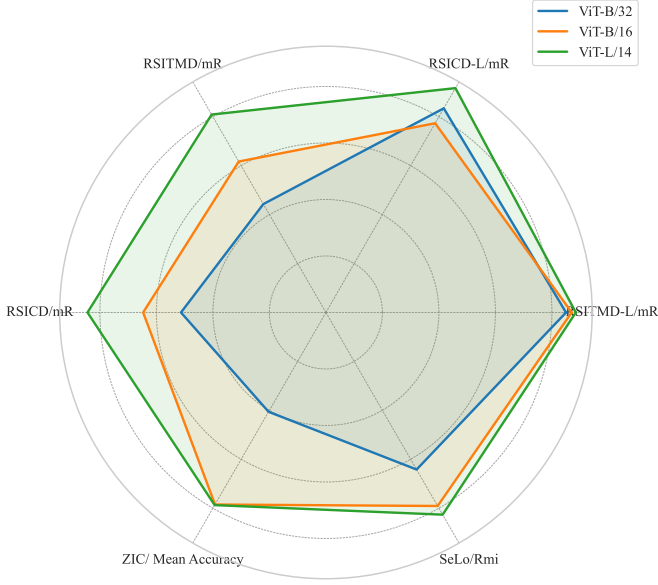


Fig. 9. Comparison of downstream task performance for models of different sizes.

helps the model capture richer local features, thereby gaining an advantage in tasks that require detailed perception, such as retrieval and localization. Furthermore, after training with long text, ViT-B/16 strikes a good balance between large-batch contrastive learning, rich semantic information injection, and relatively fine visual resolution, achieving overall superior performance.

Meanwhile, ViT-L/14, with a larger model capacity, benefits from long text training and further enhances the model's ability to express complex cross-modal semantics, resulting in performance improvements across all downstream tasks. This suggests that when both text length and image detail are fully exploited, the model can better utilize multimodal information to achieve more accurate retrieval and classification.

#### 6) Influence of Using the First Sentence and Short text:

In this comparative experiment, two strategies were adopted to process short texts: the first strategy follows the original training approach of Long-CLIP, where the first sentence of the long text is used as the short text (First Text); the second strategy introduces an independent short text (Short Text). As shown in **TABLE. VIII**, the mR values for the two strategies are similar in the ZCRL task. However, in tasks such as ZCRS, ZIC, and SeLo, the strategy using dedicated short texts achieves superior performance in most metrics. This suggests that while the summary description of the first sentence provides some semantic information for cross-modal retrieval, it may be too sparse to fully capture the detailed information required by the image. In contrast, directly using an additional short text allows for more effective and fine-grained guidance of the image, resulting in better performance in fine-grained retrieval and image understanding tasks.

#### 7) Influence of Long Text and Short Text Loss Weight Ratio:

**Fig. 10** presents the results of downstream tasks under different loss weight ratios. In the ZCRL and ZIC tasks, appropriately increasing the weight of the long text

TABLE VIII  
INFLUENCE OF USING THE FIRST SENTENCE OF LONG TEXT AS A SHORT TEXT VERSUS USING ADDITIONAL SHORT TEXTS.

Short Text	ZCRL	ZCRS	ZIC	SeLo
First Text	64.82	34.36	71.12	0.7396
Short Text	64.79	36.17	75.70	0.7582

helps to enhance semantic alignment, enabling the model to better capture the global information of remote sensing images, thereby improving cross-modal retrieval and classification performance. In the ZCRS task, however, although short text is crucial for fine-grained matching, excessively high short text weights (such as 4:6, 3:7, 2:8, and 1:9) lead to a decline in retrieval performance, suggesting that over-reliance on short text may impair the model's understanding of overall semantic information. Furthermore, in the SeLo task, although the 5:5 weight ratio achieves the highest Rmi, the 8:2 ratio still maintains a high Rmi, indicating that this ratio does not significantly impact spatial semantic alignment ability while preserving overall performance in other tasks.

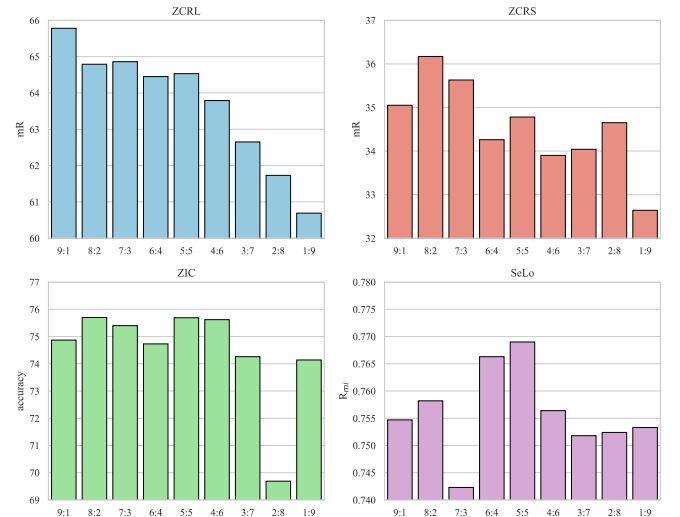


Fig. 10. Results of varying loss weights between long text and short text at different ratios.

From the perspectives of training stability and task adaptability, the 8:2 weight ratio achieves the best balance between global information from long text and fine-grained alignment from short text. The long text provides rich contextual information, improving the model's performance in ZCRL and ZIC tasks, while the short text enhances the precise matching ability of images, playing a key role in ZCRS tasks. However, a short text weight that is too high may weaken global semantic understanding and impact cross-modal alignment ability, while an overly high long text weight could reduce short text retrieval accuracy. Therefore, the 8:2 weight ratio not only optimizes retrieval and classification task performance but also ensures model stability and generalization ability, making it the optimal configuration for training LRSCLIP.

## 8) Influence of Fine-tuning from Long-CLIP or CLIP:

**TABLE. IX** compares the impact of fine-tuning based on Long-CLIP and CLIP on the performance of LRSCLIP in various tasks. The results show that Long-CLIP performs slightly better in the ZCRL task, while CLIP outperforms in the ZCRS and ZIC tasks. Additionally, in the SeLo task, the performance of both models is comparable, indicating that the choice of the initial model has minimal impact on this task. Overall, the fine-tuned weights from CLIP demonstrate stronger generalization capabilities for short-text retrieval and classification tasks while still maintaining competitiveness in long-text retrieval and semantic localization tasks. Therefore, fine-tuning based on CLIP was ultimately chosen to ensure the balanced performance of LRSCLIP across different tasks.

TABLE IX  
INFLUENCE OF FINE-TUNING FROM LONG-CLIP OR CLIP.

from	ZCRL	ZCRS	ZIC	SeLo
Long-CLIP	65.45	34.16	73.40	0.7578
CLIP	64.79	36.17	75.70	0.7582

## VI. CONCLUSION AND DISCUSSION

In this study, we constructed the LRS2M dataset and trained the LRSCLIP model, marking an important step in remote sensing vision-language foundation model. However, several areas remain to be explored and improved.

Firstly, although LRSCLIP performs excellently on multiple zero-shot tasks, there is still room for optimization. The existing techniques used in LRSCLIP may not fully capture the complex relationships between long text semantics and remote sensing image features at a fine-grained level. Future research could focus on designing more advanced architectures or algorithms to enhance the interaction between modalities. For example, exploring neural network structures that can better handle long-term dependencies in long texts and their corresponding spatial relationships in remote sensing images.

Secondly, while the construction of the LRS2M dataset is innovative in providing both short and long texts, it can still be further refined. The current data sources and annotation methods have limitations. We could explore more diverse data collection channels to cover a wider range of remote sensing scenarios. Additionally, the annotation process can be optimized to ensure more accurate and detailed descriptions, which will help the model undergo better training.

In terms of model evaluation, the current zero-shot task set is valuable but can be expanded. There is potential to design more complex and realistic evaluation metrics that better reflect the model's performance in remote sensing applications—for example, considering the uncertainty and contextual information of remote sensing data during evaluation rather than relying solely on existing recall-based and accuracy-based metrics.

Finally, we should extend the application of LRSCLIP and similar models to more remote sensing downstream tasks. So far, we have primarily focused on cross-modal retrieval,

zero-shot classification, and semantic localization tasks. Future work could explore the performance of these models in tasks such as multi-temporal remote sensing data analysis for environmental monitoring, 3D object detection in urban remote sensing scenes, and real-time semantic segmentation for autonomous remote sensing systems. These explorations will not only expand the practical application range of remote sensing vision-language models but also promote the development of the entire remote sensing research field.

## APPENDIX

### A. The Generation Instructions and Data Format of LRS2M

2. Long Text → Short Text
<b>USER:</b> The aerial image shows a rural road scene. The road is a two-lane asphalt road with a white stripe down the middle. It is surrounded by trees, which are mostly green but some are changing to fall colors. There is a small clearing on the left side of the road, which is mostly grass. There is a white house with a red roof on the right side of the road, surrounded by trees. There is also a white truck with a red stripe on the road, in the middle of the image. Summarize this image caption in 20 words or less.
<b>ASSISTANT:</b> A rural road scene with trees, a house, and a truck on an asphalt road with a stripe.
3. Short Text → Long Text
<b>USER:</b> Slice of a remote sensing image: <image>This is a brief description of this remote sensing image title: 'this is a satellite image, shot in Fall, captures the essence of non-irrigated arable land, complex cultivation patterns, transitional woodland/shrub' and is associated with utm zone 29N and is timestamped 11 o'clock, October 2, 2017. a clear view of an aerial view of a desert landscape Summarize and generate a long text image caption for the provided short text description, approximately 150 words, including the following content: 1. Main ground objects in satellite image 2. The objects attribute of the object mainly include color, position, etc. 3. Positional relationship between objects 4. Do not provide any text unrelated to image caption Image Caption:

<b>ASSISTANT:</b> The image is a slice of a remote sensing image with a single road and a single building visible. The road is a long line of vehicles moving along a paved surface. The building is a small rectangular structure with a blue roof, surrounded by greenery. The grassland is a large expanse of green vegetation, while the woodland is a dense collection of trees. The road is positioned in the middle of the image, with the building to the right and the grassland and woodland to the right and bottom. The objects in the image are all in close proximity to each other, creating a compact and lively scene. The color of the road is gray, the building is blue, and the grassland and woodland are green. The position of the objects in the image is as follows: the road is at the center, the building is to the right and the bottom, and the grassland and woodland are to the left and bottom. The objects in the image are all in close proximity to each other, creating a compact and lively scene.
4. Vector Label → Long Text → Short Text
<b>USER:</b> Slice of a remote sensing image: <image>This is a slice of a remote sensing image, and the following is a dictionary of the features and their quantity information contained in this image: 'roads': 1, 'grassland': 2, 'Woodland': 1, 'building': 1) Summarize and generate a long text image caption for the provided dictionary, approximately 150 words, including the following content: 1. Main ground objects in satellite image 2. The objects attribute of the object mainly include color, position, etc. 3. Positional relationship between objects 4. Do not provide any text unrelated to image caption Image Caption:

<b>ASSISTANT:</b> The image is a slice of a remote sensing image with a single road and a single building visible. The road is a long line of vehicles moving along a paved surface. The building is a small rectangular structure with a blue roof, surrounded by greenery. The grassland is a large expanse of green vegetation, while the woodland is a dense collection of trees. The road is positioned in the middle of the image, with the building to the right and the grassland and woodland to the right and bottom. The objects in the image are all in close proximity to each other, creating a compact and lively scene. The color of the road is gray, the building is blue, and the grassland and woodland are green.
<b>USER:</b> The image is a slice of a remote sensing image with a single road and a single building visible. The road is a long line of vehicles moving along a paved surface. The building is a small rectangular structure with a blue roof, surrounded by greenery. The grassland is a large expanse of green vegetation, while the woodland is a dense collection of trees. The road is positioned in the middle of the image, with the building to the right and the grassland and woodland to the right and bottom. The objects in the image are all in close proximity to each other, creating a compact and lively scene. The color of the road is gray, the building is blue, and the grassland and woodland are green. Summarize the description of this satellite image in about 20 words.
<b>ASSISTANT:</b> A satellite image shows a road with vehicles, a blue-roofed building, green grassland, and a dense woodland.

Fig. 11. Specific Generation Instructions Examples for LRS2M.

We introduce the image captioning generation instructions for LRS2M. Among the four collection methods of LRS2M, the first method directly collects image caption data from open-source datasets, so we will focus on the latter three methods. The second method involves directly integrating pre-labeled long-text captions with a summarization instruction such as "Summarize this image caption in 20 words or less," which is then input into the LLM. Since the content provided by the long-text captions is already sufficiently detailed, no additional image input is required. The third method combines labeled short-text image captions with specific generation instructions, along with the image data, and inputs them into the MLLM. The purpose of including short-text captions here is to prevent semantic bias during MLLM inference. The generation instructions request that the long text output include information on the main ground objects, object attributes, and

positional relationships in the remote sensing images. The fourth method involves using vector labels and their counts as semantic anchors to aid in understanding and identifying specific elements of the remote sensing images. The long-text and short-text image captions are then generated sequentially using the third and second methods, respectively. The image captions will be stored in the JSON format as shown in [Fig. 12](#).

```
{
  "filename": "DIOR_16197.jpg",
  "short_caption": [
    {
      "from": "Det-10",
      "value": "A trainstation in the middle of the picture."
    }
  ],
  "long_caption": [
    {
      "from": "Qwen2-VL",
      "value": "The image depicts a remote sensing view of a train station, ... ..."
    }
  ]
}
```

Fig. 12. The Data Format of LRS2M.

### B. The Optimizer Settings

The optimizer settings used for training are shown in [TABLE X](#).

TABLE X  
OPTIMIZER SETTINGS

name	value
optimizer	SGD
learning rate	3.0e-4
momentum	0.9
dampening	0.1

### ACKNOWLEDGMENTS

This research was funded by the National Key R&D Program of China under grant number 2021YFB3900504.

### REFERENCES

- [1] K. He, X. Chen, S. Xie, Y. Li, P. Dollár, and R. Girshick, "Masked autoencoders are scalable vision learners," in *Proceedings of the IEEE/CVF conference on computer vision and pattern recognition*, 2022, pp. 16 000–16 009.
- [2] A. Kirillov, E. Mintun, N. Ravi, H. Mao, C. Rolland, L. Gustafson, T. Xiao, S. Whitehead, A. C. Berg, W.-Y. Lo *et al.*, "Segment anything," in *Proceedings of the IEEE/CVF international conference on computer vision*, 2023, pp. 4015–4026.
- [3] M. Caron, H. Touvron, I. Misra, H. Jégou, J. Mairal, P. Bojanowski, and A. Joulin, "Emerging properties in self-supervised vision transformers," in *Proceedings of the IEEE/CVF international conference on computer vision*, 2021, pp. 9650–9660.
- [4] M. Oquab, T. Daract, T. Moutakanni, H. Vo, M. Szafraniec, V. Khalidov, P. Fernandez, D. Haziza, F. Massa, A. El-Nouby *et al.*, "Dinov2: Learning robust visual features without supervision," *arXiv preprint arXiv:2304.07193*, 2023.
- [5] X. Kong and X. Zhang, "Understanding masked image modeling via learning occlusion invariant feature," in *Proceedings of the IEEE/CVF Conference on Computer Vision and Pattern Recognition*, 2023, pp. 6241–6251.
- [6] J. Devlin, M.-W. Chang, K. Lee, and K. Toutanova, "Bert: Pre-training of deep bidirectional transformers for language understanding," in *Proceedings of the 2019 conference of the North American chapter of the association for computational linguistics: human language technologies, volume 1 (long and short papers)*, 2019, pp. 4171–4186.
- [7] A. Dubey, A. Jauhri, A. Pandey, A. Kadian, A. Al-Dahle, A. Letman, A. Mathur, A. Schelten, A. Yang, A. Fan *et al.*, "The llama 3 herd of models," *arXiv preprint arXiv:2407.21783*, 2024.
- [8] T. Brown, B. Mann, N. Ryder, M. Subbiah, J. D. Kaplan, P. Dhariwal, A. Neelakantan, P. Shyam, G. Sastry, A. Askell *et al.*, "Language models are few-shot learners," *Advances in neural information processing systems*, vol. 33, pp. 1877–1901, 2020.
- [9] Y. Zhou, L. Feng, Y. Ke, X. Jiang, J. Yan, X. Yang, and W. Zhang, "Towards vision-language geo-foundation model: A survey," *arXiv preprint arXiv:2406.09385*, 2024.
- [10] A. Radford, J. W. Kim, C. Hallacy, A. Ramesh, G. Goh, S. Agarwal, G. Sastry, A. Askell, P. Mishkin, J. Clark *et al.*, "Learning transferable visual models from natural language supervision," in *International conference on machine learning*. PMLR, 2021, pp. 8748–8763.
- [11] J. Li, D. Li, C. Xiong, and S. Hoi, "Blip: Bootstrapping language-image pre-training for unified vision-language understanding and generation," in *International conference on machine learning*. PMLR, 2022, pp. 12 888–12 900.
- [12] J. Li, D. Li, S. Savarese, and S. Hoi, "Blip-2: Bootstrapping language-image pre-training with frozen image encoders and large language models," in *International conference on machine learning*. PMLR, 2023, pp. 19 730–19 742.
- [13] G. Kwon, Z. Cai, A. Ravichandran, E. Bas, R. Bhotika, and S. Soatto, "Masked vision and language modeling for multi-modal representation learning," *arXiv preprint arXiv:2208.02131*, 2022.
- [14] Z. Li, X. Wu, H. Du, H. Nghiem, and G. Shi, "Benchmark evaluations, applications, and challenges of large vision language models: A survey," *arXiv preprint arXiv:2501.02189*, 2025.
- [15] F. Liu, D. Chen, Z. Guan, X. Zhou, J. Zhu, Q. Ye, L. Fu, and J. Zhou, "Remoteclip: A vision language foundation model for remote sensing," *IEEE Transactions on Geoscience and Remote Sensing*, 2024.
- [16] Z. Zhang, T. Zhao, Y. Guo, and J. Yin, "Rs5m and georsclip: A large scale vision-language dataset and a large vision-language model for remote sensing," *IEEE Transactions on Geoscience and Remote Sensing*, 2024.
- [17] K. Kuckreja, M. S. Danish, M. Naseer, A. Das, S. Khan, and F. S. Khan, "Geochat: Grounded large vision-language model for remote sensing," in *Proceedings of the IEEE/CVF Conference on Computer Vision and Pattern Recognition*, 2024, pp. 27 831–27 840.
- [18] M. M. Al Rahhal, Y. Bazi, H. Elgibreen, and M. Zuair, "Vision-language models for zero-shot classification of remote sensing images," *Applied Sciences*, vol. 13, no. 22, p. 12462, 2023.
- [19] Y. Zhou, M. Lan, X. Li, Y. Ke, X. Jiang, L. Feng, and W. Zhang, "Geoground: A unified large vision-language model for remote sensing visual grounding," *arXiv preprint arXiv:2411.11904*, 2024.
- [20] U. Mall, C. Phoo, M. Liu, C. Vondrick, B. Hariharan, and K. Bala, "Remote sensing vision-language foundation models without annotations via ground remote alignment. arxiv 2023," *arXiv preprint arXiv:2312.06960*.
- [21] K. Li, R. Liu, X. Cao, X. Bai, F. Zhou, D. Meng, and Z. Wang, "Segearth-ov: Towards training-free open-vocabulary segmentation for remote sensing images," *arXiv preprint arXiv:2410.01768*, 2024.
- [22] K. Li, X. Cao, Y. Deng, C. Pang, Z. Xin, D. Meng, and Z. Wang, "Dynamicearth: How far are we from open-vocabulary change detection?" *arXiv preprint arXiv:2501.12931*, 2025.
- [23] K. Li, X. Cao, Y. Deng, J. Song, J. Liu, D. Meng, and Z. Wang, "Semicdvl: Visual-language model guidance makes better semi-supervised change detector," *IEEE Transactions on Geoscience and Remote Sensing*, 2024.
- [24] H. Lin, D. Hong, S. Ge, C. Luo, K. Jiang, H. Jin, and C. Wen, "Rs-moe: Mixture of experts for remote sensing image captioning and visual question answering," *arXiv preprint arXiv:2411.01595*, 2024.
- [25] T. Abdullah, Y. Bazi, M. M. Al Rahhal, M. L. Mekhafii, L. Rangarajan, and M. Zuair, "Textrs: Deep bidirectional triplet network for matching text to remote sensing images," *Remote Sensing*, vol. 12, no. 3, p. 405, 2020.
- [26] X. Lu, B. Wang, X. Zheng, and X. Li, "Exploring models and data for remote sensing image caption generation," *IEEE Transactions on Geoscience and Remote Sensing*, vol. 56, no. 4, pp. 2183–2195, 2017.

[27] Z. Yuan, W. Zhang, K. Fu, X. Li, C. Deng, H. Wang, and X. Sun, “Exploring a fine-grained multiscale method for cross-modal remote sensing image retrieval,” *arXiv preprint arXiv:2204.09868*, 2022.

[28] Y. Yang and S. Newsam, “Bag-of-visual-words and spatial extensions for land-use classification,” in *Proceedings of the 18th SIGSPATIAL international conference on advances in geographic information systems*, 2010, pp. 270–279.

[29] B. Qu, X. Li, D. Tao, and X. Lu, “Deep semantic understanding of high resolution remote sensing image,” in *2016 International conference on computer, information and telecommunication systems (Cits)*. IEEE, 2016, pp. 1–5.

[30] W. Wu, K. Zheng, S. Ma, F. Lu, Y. Guo, Y. Zhang, W. Chen, Q. Guo, Y. Shen, and Z.-J. Zha, “Lotlip: Improving language-image pre-training for long text understanding,” *arXiv preprint arXiv:2410.05249*, 2024.

[31] B. Zhang, P. Zhang, X. Dong, Y. Zang, and J. Wang, “Long-clip: Unlocking the long-text capability of clip,” in *European Conference on Computer Vision*. Springer, 2024, pp. 310–325.

[32] F. Pourpanah, M. Abdar, Y. Luo, X. Zhou, R. Wang, C. P. Lim, X.-Z. Wang, and Q. J. Wu, “A review of generalized zero-shot learning methods,” *IEEE transactions on pattern analysis and machine intelligence*, vol. 45, no. 4, pp. 4051–4070, 2022.

[33] Z. Yuan, W. Zhang, C. Li, Z. Pan, Y. Mao, J. Chen, S. Li, H. Wang, and X. Sun, “Learning to evaluate performance of multi-modal semantic localization,” *arXiv preprint arXiv:2209.06515*, 2022.

[34] A. Xiao, W. Xuan, J. Wang, J. Huang, D. Tao, S. Lu, and N. Yokoya, “Foundation models for remote sensing and earth observation: A survey,” *arXiv preprint arXiv:2410.16602*, 2024.

[35] F. Schroff, D. Kalenichenko, and J. Philbin, “Facenet: A unified embedding for face recognition and clustering,” in *Proceedings of the IEEE conference on computer vision and pattern recognition*, 2015, pp. 815–823.

[36] A. v. d. Oord, Y. Li, and O. Vinyals, “Representation learning with contrastive predictive coding,” *arXiv preprint arXiv:1807.03748*, 2018.

[37] D. Muhtar, Z. Li, F. Gu, X. Zhang, and P. Xiao, “Lhrs-bot: Empowering remote sensing with vgi-enhanced large multimodal language model,” in *European Conference on Computer Vision*. Springer, 2024, pp. 440–457.

[38] X. Zhai, B. Mustafa, A. Kolesnikov, and L. Beyer, “Sigmoid loss for language image pre-training,” in *Proceedings of the IEEE/CVF international conference on computer vision*, 2023, pp. 11975–11986.

[39] N. Mu, A. Kirillov, D. Wagner, and S. Xie, “Slip: Self-supervision meets language-image pre-training,” in *European conference on computer vision*. Springer, 2022, pp. 529–544.

[40] Y. Huang, J. Tang, Z. Chen, R. Zhang, X. Zhang, W. Chen, Z. Zhao, Z. Zhao, T. Lv, Z. Hu *et al.*, “Structure-clip: Towards scene graph knowledge to enhance multi-modal structured representations,” in *Proceedings of the AAAI conference on artificial intelligence*, vol. 38, no. 3, 2024, pp. 2417–2425.

[41] C. Zhou, C. C. Loy, and B. Dai, “Extract free dense labels from clip,” in *European Conference on Computer Vision*. Springer, 2022, pp. 696–712.

[42] M. Tschannen, B. Mustafa, and N. Houlsby, “Clippo: Image-and-language understanding from pixels only,” in *Proceedings of the IEEE/CVF Conference on Computer Vision and Pattern Recognition*, 2023, pp. 11006–11017.

[43] Y. Zhong, J. Yang, P. Zhang, C. Li, N. Codella, L. H. Li, L. Zhou, X. Dai, L. Yuan, Y. Li *et al.*, “Regionclip: Region-based language-image pretraining,” in *Proceedings of the IEEE/CVF conference on computer vision and pattern recognition*, 2022, pp. 16793–16803.

[44] L. Xiao, X. Yang, F. Peng, M. Yan, Y. Wang, and C. Xu, “Clip-vg: Self-paced curriculum adapting of clip for visual grounding,” *IEEE Transactions on Multimedia*, vol. 26, pp. 4334–4347, 2023.

[45] S. Kim, M. Kang, D. Kim, J. Park, and S. Kwak, “Extending clip’s image-text alignment to referring image segmentation,” *arXiv preprint arXiv:2306.08498*, 2023.

[46] Z. Wang, R. Prabha, T. Huang, J. Wu, and R. Rajagopal, “Skyscript: A large and semantically diverse vision-language dataset for remote sensing,” in *Proceedings of the AAAI Conference on Artificial Intelligence*, vol. 38, no. 6, 2024, pp. 5805–5813.

[47] V. Vivanco Cepeda, G. K. Nayak, and M. Shah, “Geoclip: Clip-inspired alignment between locations and images for effective worldwide geo-localization,” *Advances in Neural Information Processing Systems*, vol. 36, pp. 8690–8701, 2023.

[48] K. Klemmer, E. Rolf, C. Robinson, L. Mackey, and M. Rußwurm, “Satclip: Global, general-purpose location embeddings with satellite imagery,” *arXiv preprint arXiv:2311.17179*, 2023.

[49] K. Zheng, Y. Zhang, W. Wu, F. Lu, S. Ma, X. Jin, W. Chen, and Y. Shen, “Dreamlip: Language-image pre-training with long captions,” in *European Conference on Computer Vision*. Springer, 2024, pp. 73–90.

[50] Y. K. Jang, J. Kang, Y. J. Lee, and D. Kim, “Mate: Meet at the embedding—connecting images with long texts,” *arXiv preprint arXiv:2407.09541*, 2024.

[51] I. Najdenkoska, M. M. Derakhshani, Y. M. Asano, N. van Noord, M. Worring, and C. G. Snoek, “Tulip: Token-length upgraded clip,” *arXiv preprint arXiv:2410.10034*, 2024.

[52] Y. Long, G.-S. Xia, S. Li, W. Yang, M. Y. Yang, X. X. Zhu, L. Zhang, and D. Li, “On creating benchmark dataset for aerial image interpretation: Reviews, guidances, and million-aid,” *IEEE Journal of selected topics in applied earth observations and remote sensing*, vol. 14, pp. 4205–4230, 2021.

[53] C. Pang, X. Weng, J. Wu, J. Li, Y. Liu, J. Sun, W. Li, S. Wang, L. Feng, G.-S. Xia *et al.*, “Vhm: Versatile and honest vision language model for remote sensing image analysis,” *arXiv preprint arXiv:2403.20213*, 2024.

[54] S. P. Mohanty, J. Czakon, K. A. Kaczmarek, A. Pyskir, P. Tarasiewicz, S. Kunwar, J. Rohrbach, D. Luo, M. Prasad, S. Fleer *et al.*, “Deep learning for understanding satellite imagery: An experimental survey,” *Frontiers in Artificial Intelligence*, vol. 3, p. 534696, 2020.

[55] A. Yang, B. Yang, B. Zhang, B. Hui, B. Zheng, B. Yu, C. Li, D. Liu, F. Huang, H. Wei *et al.*, “Qwen2. 5 technical report,” *arXiv preprint arXiv:2412.15115*, 2024.

[56] L. Liu and H. Li, “Lending orientation to neural networks for cross-view geo-localization,” in *Proceedings of the IEEE/CVF conference on computer vision and pattern recognition*, 2019, pp. 5624–5633.

[57] Z. Cai, M. Cao, H. Chen, K. Chen, X. Chen, X. Chen, Z. Chen, Z. Chen, P. Chu *et al.*, “Internlm2 technical report,” *arXiv preprint arXiv:2403.17297*, 2024.

[58] M. Zhai, Z. Bessinger, S. Workman, and N. Jacobs, “Predicting ground-level scene layout from aerial imagery,” in *Proceedings of the IEEE Conference on Computer Vision and Pattern Recognition*, 2017, pp. 867–875.

[59] G. Christie, N. Fendley, J. Wilson, and R. Mukherjee, “Functional map of the world,” in *Proceedings of the IEEE Conference on Computer Vision and Pattern Recognition*, 2018, pp. 6172–6180.

[60] J. Wang, Z. Zheng, A. Ma, X. Lu, and Y. Zhong, “Loveda: A remote sensing land-cover dataset for domain adaptive semantic segmentation,” *arXiv preprint arXiv:2110.08733*, 2021.

[61] T. GLM, A. Zeng, B. Xu, B. Wang, C. Zhang, D. Yin, D. Zhang, D. Rojas, G. Feng, H. Zhao *et al.*, “Chatglm: A family of large language models from glm-130b to glm-4 all tools,” *arXiv preprint arXiv:2406.12793*, 2024.

[62] G. Sumbul, M. Charfuelan, B. Demir, and V. Markl, “Bigearthnet: A large-scale benchmark archive for remote sensing image understanding,” in *IGARSS 2019-2019 IEEE international geoscience and remote sensing symposium*. IEEE, 2019, pp. 5901–5904.

[63] P. Wang, S. Bai, S. Tan, S. Wang, Z. Fan, J. Bai, K. Chen, X. Liu, J. Wang, W. Ge *et al.*, “Qwen2-vl: Enhancing vision-language model’s perception of the world at any resolution,” *arXiv preprint arXiv:2409.12191*, 2024.

[64] B. Li, Y. Zhang, D. Guo, R. Zhang, F. Li, H. Zhang, K. Zhang, P. Zhang, Y. Li, Z. Liu *et al.*, “Llava-onevision: Easy visual task transfer,” *arXiv preprint arXiv:2408.03326*, 2024.

[65] S. Vujasinović, S. Becker, T. Breuer, S. Bullinger, N. Scherer-Negenborn, and M. Arens, “Integration of the 3d environment for uav onboard visual object tracking,” *Applied Sciences*, vol. 10, no. 21, p. 7622, 2020.

[66] M.-R. Hsieh, Y.-L. Lin, and W. H. Hsu, “Drone-based object counting by spatially regularized regional proposal network,” in *Proceedings of the IEEE international conference on computer vision*, 2017, pp. 4145–4153.

[67] K. Li, G. Wan, G. Cheng, L. Meng, and J. Han, “Object detection in optical remote sensing images: A survey and a new benchmark,” *ISPRS journal of photogrammetry and remote sensing*, vol. 159, pp. 296–307, 2020.

[68] G.-S. Xia, X. Bai, J. Ding, Z. Zhu, S. Belongie, J. Luo, M. Datcu, M. Pelillo, and L. Zhang, “Dota: A large-scale dataset for object detection in aerial images,” in *Proceedings of the IEEE conference on computer vision and pattern recognition*, 2018, pp. 3974–3983.

[69] Y. Zhang, Y. Yuan, Y. Feng, and X. Lu, “Hierarchical and robust convolutional neural network for very high-resolution remote sensing object detection,” *IEEE Transactions on Geoscience and Remote Sensing*, vol. 57, no. 8, pp. 5535–5548, 2019.

[70] Z. Liu, L. Yuan, L. Weng, and Y. Yang, “A high resolution optical satellite image dataset for ship recognition and some new baselines,” in *International conference on pattern recognition applications and methods*, vol. 2. SciTePress, 2017, pp. 324–331.

[71] H. Chen and Z. Shi, “A spatial-temporal attention-based method and a new dataset for remote sensing image change detection,” *Remote sensing*, vol. 12, no. 10, p. 1662, 2020.

[72] W. Sun, L. Dai, X. Zhang, P. Chang, and X. He, “Rsod: Real-time small object detection algorithm in uav-based traffic monitoring,” *Applied Intelligence*, pp. 1–16, 2022.

[73] A. Robicquet, A. Sadeghian, A. Alahi, and S. Savarese, “Learning social etiquette: Human trajectory understanding in crowded scenes,” in *Computer Vision–ECCV 2016: 14th European Conference, Amsterdam, The Netherlands, October 11–14, 2016, Proceedings, Part VIII 14*. Springer, 2016, pp. 549–565.

[74] P. Zhu, L. Wen, X. Bian, H. Ling, and Q. Hu, “Vision meets drones: A challenge,” *arXiv preprint arXiv:1804.07437*, 2018.

[75] S. Waqas Zamir, A. Arora, A. Gupta, S. Khan, G. Sun, F. Shahbaz Khan, F. Zhu, L. Shao, G.-S. Xia, and X. Bai, “isaid: A large-scale dataset for instance segmentation in aerial images,” in *Proceedings of the IEEE/CVF conference on computer vision and pattern recognition workshops*, 2019, pp. 28–37.

[76] “2D Semantic Label - Vaihingen.” [Online]. Available: <https://www.isprs.org/education/benchmarks/UrbanSemLab/2d-sem-label-vaihingen.aspx>

[77] “2D Semantic Labeling Contest - Potsdam.” [Online]. Available: <https://www.isprs.org/education/benchmarks/UrbanSemLab/2d-sem-label-potsdam.aspx>

[78] K. He, X. Zhang, S. Ren, and J. Sun, “Deep residual learning for image recognition,” in *Proceedings of the IEEE conference on computer vision and pattern recognition*, 2016, pp. 770–778.

[79] A. Dosovitskiy, L. Beyer, A. Kolesnikov, D. Weissenborn, X. Zhai, T. Unterthiner, M. Dehghani, M. Minderer, G. Heigold, S. Gelly *et al.*, “An image is worth 16x16 words: Transformers for image recognition at scale,” *arXiv preprint arXiv:2010.11929*, 2020.

[80] S. Zhang, Y. Xu, N. Usuyama, J. Bagga, R. Tinn, S. Preston, R. Rao, M. Wei, N. Valluri, C. Wong *et al.*, “Large-scale domain-specific pretraining for biomedical vision-language processing,” *arXiv preprint arXiv:2303.00915*, vol. 2, no. 3, p. 6, 2023.

[81] E. J. Hu, Y. Shen, P. Wallis, Z. Allen-Zhu, Y. Li, S. Wang, L. Wang, W. Chen *et al.*, “Lora: Low-rank adaptation of large language models,” *ICLR*, vol. 1, no. 2, p. 3, 2022.

[82] G. Cheng, J. Han, and X. Lu, “Remote sensing image scene classification: Benchmark and state of the art,” *Proceedings of the IEEE*, vol. 105, no. 10, pp. 1865–1883, 2017.

[83] P. Helber, B. Bischke, A. Dengel, and D. Borth, “Eurosat: A novel dataset and deep learning benchmark for land use and land cover classification,” *IEEE Journal of Selected Topics in Applied Earth Observations and Remote Sensing*, vol. 12, no. 7, pp. 2217–2226, 2019.

[84] W. Zhou, S. Newsam, C. Li, and Z. Shao, “Patternnet: A benchmark dataset for performance evaluation of remote sensing image retrieval,” *ISPRS journal of photogrammetry and remote sensing*, vol. 145, pp. 197–209, 2018.

[85] B. Zhao, Y. Zhong, G.-S. Xia, and L. Zhang, “Dirichlet-derived multiple topic scene classification model for high spatial resolution remote sensing imagery,” *IEEE Transactions on Geoscience and Remote Sensing*, vol. 54, no. 4, pp. 2108–2123, 2015.

[86] Q. Wang, S. Liu, J. Chanussot, and X. Li, “Scene classification with recurrent attention of vhr remote sensing images,” *IEEE Transactions on Geoscience and Remote Sensing*, vol. 57, no. 2, pp. 1155–1167, 2018.

[87] L. Zhao, P. Tang, and L. Huo, “Feature significance-based multibag-of-visual-words model for remote sensing image scene classification,” *Journal of Applied Remote Sensing*, vol. 10, no. 3, pp. 035 004–035 004, 2016.

[88] M. Yu, H. Yuan, J. Chen, C. Hao, Z. Wang, Z. Yuan, and B. Lu, “Selo v2: Toward for higher and faster semantic localization,” *IEEE Geoscience and Remote Sensing Letters*, vol. 20, pp. 1–5, 2023.



**Weizhi Chen** received a bachelor's degree in engineering, resource exploration engineering from China University of Mining and Technology, Xuzhou, China, in 2023. He is currently pursuing a master's degree with University of Chinese Academy of Sciences, Beijing, China.

His research interests include remote sensing vision-language model, encompassing foundation model and multimodal large language model.



**Zhihao Xi** received the Ph.D. degree from the Aerospace Information Research Institute, Chinese Academy of Sciences, Beijing, China, in 2024.

He is currently an Assistant Professor with the Aerospace Information Research Institute, CAS. His research interests include computer vision, domain adaptation, and remote sensing image interpretation.



**Jingbo Chen** received the Ph.D. degree in cartography and geographic information systems from the Institute of Remote Sensing Applications, Chinese Academy of Sciences, Beijing, China, in 2011.

He is currently a Professor with the Aerospace Information Research Institute, Chinese Academy of Sciences. His research interests cover intelligent remote sensing analysis, integrated application of communication, navigation, and remote sensing.



**Diyou Liu** received the Ph.D. degree in Agricultural Information Technology, College of Land Science and Technology, China Agricultural University in 2021.

He is currently a Special Research Assistant at Aerospace Information Research Institute, Chinese Academy of Sciences, Beijing, China. His research focuses on the production of cartographic-level vector element data using intelligent interpretation methods from high-resolution remote sensing imagery.



**Yupeng Deng** received the Ph.D. degree from the Aerospace Information Research Institute, Chinese Academy of Sciences, Beijing, China, in 2023.

He is currently a Special Assistant Professor with the Aerospace Information Research Institute, CAS. His research interests include computer vision, remote sensing intelligent mapping and change detection.



**Kai Li** received a bachelor's degree in engineering, spatial information and digital technology from University of Electronic Science and Technology of China, Chengdu, China, in 2021. He is currently pursuing a PhD degree with University of Chinese Academy of Sciences, Beijing, China.

His research interests include remote sensing, computer vision, and machine learning.



**Jiansheng Chen** received the Ph.D. degree in signal and information processing from Institute of remote sensing applications, Chinese Academy of Sciences, Beijing, China, in 2012.

He is currently working with Aerospace Information Research Institute, Chinese Academy of Sciences. His research interests include remote sensing intelligent interpretation and big data governance.



**Yu Meng** received the Ph.D. degree in signal and information processing from the Institute of Remote Sensing Applications, Chinese Academy of Sciences, Beijing, China, in 2008.

She is currently a Professor at the Aerospace Information Research Institute, Chinese Academy of Sciences. Her research interests include intelligent interpretation of remote sensing images, remote sensing time-series signal processing, and big spatial-temporal data application.

Dr Meng serves as an editor and board member of the National Remote Sensing Bulletin, Journal of Image and Graphics.



**Yuman Feng** is currently an undergraduate student majoring in Cybersecurity and Law Enforcement at the School of Information Network Security, People's Public Security University of China. During the holidays, she interned at the Institute of Air and Space Information, Chinese Academy of Sciences. Her research interests include mathematical modeling, artificial intelligence, and network attack and defense.